HHS Public Access

Author manuscript

FASEB J. Author manuscript; available in PMC 2022 May 02.

Published in final edited form as:

FASEB J. 2022 January ; 36(1): e22094. doi:10.1096/fj.202101194RRR.

Alterations in sphingolipid composition and mitochondrial bioenergetics represent synergistic therapeutic vulnerabilities linked to multidrug resistance in leukemia

Kelsey H. Fisher-Wellman[1], **James T. Hagen**[1], **Miki Kassai**[2], **Li-Pin Kao**[2], **Margaret A. M. Nelson**[1], **Kelsey L. McLaughlin**[1], **Hannah S. Coalson**[1], **Todd E. Fox**[3], **Su-Fern Tan**[4], **David J. Feith**[4,5], **Mark Kester**[4,5], **Thomas P. Loughran Jr**[4,5], **David F. Claxton**[6,7], **Myles C. Cabot**[2]

[1]Department of Physiology, Brody School of Medicine, and the East Carolina Diabetes and Obesity Institute, East Carolina University, Greenville, North Carolina, USA

[2]Department of Biochemistry & Molecular Biology, Brody School of Medicine, and the East Carolina Diabetes and Obesity Institute, East Carolina University, Greenville, North Carolina, USA

[3]Department of Pharmacology, University of Virginia School of Medicine, Charlottesville, Virginia, USA

[4]Department of Medicine, Hematology/Oncology, University of Virginia School of Medicine, Charlottesville, Virginia, USA

[5]University of Virginia Cancer Center, Charlottesville, Virginia, USA

[6]Department of Medicine, Division of Hematology and Oncology, Pennsylvania State University College of Medicine, Hershey, Pennsylvania, USA

[7]Penn state Cancer Institute, Hershey, Pennsylvania, USA

Abstract

Modifications in sphingolipid (SL) metabolism and mitochondrial bioenergetics are key factors implicated in cancer cell response to chemotherapy, including chemotherapy resistance. In the present work, we utilized acute myeloid leukemia (AML) cell lines, selected to be refractory to various chemotherapeutics, to explore the interplay between SL metabolism and

Correspondence: Kelsey H. Fisher-Wellman, Department of Physiology, Brody School of Medicine, and the East Carolina Diabetes and Obesity Institute, East Carolina University, Greenville, NC 27834, USA. fisherwellmank17@ecu.edu; Myles C. Cabot, Department of Biochemistry & Molecular Biology, Brody School of Medicine, and the East Carolina Diabetes and Obesity Institute, East Carolina University, Greenville, NC 27834, USA. cabotm@ecu.edu.

AUTHORS' CONTRIBUTIONS

Kelsey H. Fisher-Wellman, James T. Hagen, Miki Kassai, Li-Pin Kao, Margaret A.M. Nelson, Kelsey L. McLaughlin, Hannah S. Coalson, Todd E. Fox, Su-Fern Tan, David J. Feith, Mark Kester, Thomas P. Loughran Jr, David F. Claxton, and Myles C. Cabot took part in the data collection and analysis. Kelsey H. Fisher-Wellman and Myles C. Cabot did the study design. Kelsey H. Fisher-Wellman and Myles C. Cabot participated in drafting and editing the manuscript. Kelsey H. Fisher-Wellman and Myles C. Cabot were responsible for the funding support. All authors read and approved the final manuscript.

DISCLOSURES

Authors declare that they have no conflicts of interest with the contents of this article. MK is Chief Medical Officer and co-founder of Keystone Nano, Inc., and TPL is a member of the scientific advisory board. TPL is on the Scientific Advisory Board and has stock options for Keystone Nano, Bioniz Therapeutics, and Dren Bio. TPL and DF received honoraria from Kymera Therapeutics.

SUPPORTING INFORMATION

Additional supporting information may be found in the online version of the article at the publisher's website.

mitochondrial biology supportive of multidrug resistance (MDR). In agreement with previous findings in cytarabine or daunorubicin resistant AML cells, relative to chemosensitive wildtype controls, HL-60 cells refractory to vincristine (HL60/VCR) presented with alterations in SL enzyme expression and lipidome composition. Such changes were typified by upregulated expression of various ceramide detoxifying enzymes, as well as corresponding shifts in ceramide, glucosylceramide, and sphingomyelin (SM) molecular species. With respect to mitochondria, despite consistent increases in both basal respiration and maximal respiratory capacity, direct interrogation of the oxidative phosphorylation (OXPHOS) system revealed intrinsic deficiencies in HL60/VCR, as well as across multiple MDR model systems. Based on the apparent requirement for augmented SL and mitochondrial flux to support the MDR phenotype, we explored a combinatorial therapeutic paradigm designed to target each pathway. Remarkably, despite minimal cytotoxicity in peripheral blood mononuclear cells (PBMC), co-targeting SL metabolism, and respiratory complex I (CI) induced synergistic cytotoxicity consistently across multiple MDR leukemia models. Together, these data underscore the intimate connection between cellular sphingolipids and mitochondrial metabolism and suggest that pharmacological intervention across both pathways may represent a novel treatment strategy against MDR.

Keywords

acute myeloid leukemia; chemotherapy resistance; HL-60 cells; mitochondrial bioenergetics; sphingolipids; vincristine

1 | BACKGROUND

A major element underlying treatment failure in cancer is chemotherapy resistance. Factors contributing to resistance include drug efflux driven by multidrug resistance (MDR) membrane transport proteins (e.g., P-glycoprotein; P-gp), drug activation/inactivation missteps, DNA damage repair, cell death inhibition (i.e., resistance to apoptosis), mutation of the target to reduce inhibitor binding, and alterations in mitochondrial bioenergetics.[1–3] These current research paradigms by and large drive the study of MDR in cancer. *Vinca* alkaloids, such as vincristine (VCR) and vinblastine (VBL), part of the World Health Organization's List of Essential Medicines, are no exception; their benefits are supplanted by upregulated expression of MDR proteins, dysfunctional apoptosis, and alterations in β-tubulin that thwart *Vinca*-associated microtubule targeting benefits. Despite these limitations, *Vinca* alkaloids are used widely in the treatment of both liquid and solid tumors, and VCR, as well as VBL, are frequent agents in combination regimens. VCR is a component in CVP (cyclophosphamide, VCR, prednisone) used in follicular B-cell lymphoma, CHOP (cyclophosphamide, doxorubicin, VCR, prednisone) used in large B-cell lymphoma, and was recently demonstrated to exert anti-leukemic effects in CD44+ acute myeloid leukemia (AML) when administered as A6 peptide-functionalized polymersomal vincristine sulfate.[4] Although VCR resistance is the main model in the present work, this study also encompasses resistance to daunorubicin and venetoclax, drugs frequently used in AML therapy.

In addition to the hallmark factors underlying chemotherapy resistance, the interplay of SL's and mitochondrial bioenergetics merits consideration. Many anticancer agents raise intracellular levels of ceramides, SL's that exhibit strong tumor-suppressing activities.[5] With respect to VCR, Olshefski and Ladisch[6] have shown that VCR exposure increases ceramide levels in leukemia cells, resulting in apoptotic responses that were intensified by blocking ceramide glycosylation. Interestingly, inhibitors of SL enzymes were recently found to interfere with energy transduction across the AML mitochondrial network, suggestive of a direct link between SL metabolism and mitochondrial bioenergetics.[7] Together, these findings raise the intriguing possibility that SL-mitochondria crosstalk may play a fundamental role in chemotherapy response and thus represent an opportunity for novel therapeutic interventions against MDR.

Herein, we utilized AML cell lines, selected to be refractory to various chemotherapeutics, to evaluate the interplay between SL metabolism and mitochondrial bioenergetics and explore the therapeutic potential of co-targeting these pathways in MDR. Consistent with prior work focused on cytarabine and daunorubicin,[8] in HL-60/VCR cells as opposed to wild-type (wt) HL-60 cells, we detail striking alterations in SL composition, highlighted by specific increases in S1P, ceramides, as well GC, and changes in levels of specific SM molecular species. These changes were accompanied by intrinsic mitochondrial remodeling that allowed for higher basal respiration and overall respiratory capacity, alongside substantial deficiencies in oxidative phosphorylation (OXPHOS). Apparent increases in respiratory capacity combined with intrinsic OXPHOS limitations were previously observed in the context of venetoclax resistance[9] and were once again observed herein for multiple MDR AML models. Based on consistent observations linking both SL and mitochondrial remodeling, therapeutic synergy was explored across both pathways. Importantly, across multiple MDR leukemia and despite minimal cytotoxicity as single agents, the combination of forced ceramide accumulation, via the addition of C6-ceramide nanoliposomes (CNL), with CI inhibition, induced synergistic cell death.

2 | MATERIALS AND METHODS

2.1 | Materials

C6-ceramide (*N*-hexanoyl-D-*erythro*-sphingosine) was from Avanti Polar Lipids, Alabaster, AL. Ceramide nanoliposomes (CNL) were a generous gift from Keystone Nano, Inc. Control (ghost) formulations included all liposomal ingredients except C6- ceramide. Propidium iodide (PI) was obtained from Life Technologies/Thermo Fisher, Carlsbad, CA. SK1-i, a SPHK1 inhibitor, was from Enzo, Farmingdale, NY. Vincristine sulfate was purchased from LC Laboratories, Woburn, MA. Daunorubicin (DNR) and venetoclax (Vclax) were from R&D Systems, Minneapolis, MN. Metformin and phenformin were purchased from Sigma. IACS-010759 was purchased from SelleckChem. com (Cat # S8731). All chemicals for mitochondrial analysis were purchased from Sigma. D-threo-1-phenyl-2-decanoylamino-3-morpholino-1-propanol (PDMP) was purchased from Cayman, Ann Arbor, MI.

2.2 | Peripheral blood mononuclear cells (PBMC)

For Peripheral blood mononuclear cells (PBMC) samples, healthy subjects, without a prior history of hematological malignancy, were recruited. Following informed consent (study ID: UMCIRB 18-001328), venous blood from the brachial region of the upper arm was collected. Collection of whole blood was performed in sodium-heparinized Cell Preparation Tubes (CPT) (BD Biosciences, Franklin Lakes, NJ) and tubes were centrifuged at 1800×*g* for 15 min. Mononuclear cells were washed in ammoniumchloride-potassium (ACK) lysis buffer to remove red blood cells and cultured for 48 h in IMDM (Thermo Fisher Scientific, Waltham, MA) supplemented with glutamine, 10% FBS, and 1% penicillin/streptomycin.

2.3 | Cell culture

The human VCR resistant (multidrug-resistant) cell line, HL-60/VCR, was developed by Safa and colleagues from HL-60/Vinc cells, originally developed by Melvin S. Center, Division of Biology, Kansas State University, Manhattan, KS, by step-wise selection to increasing concentrations of VCR.[10] Cells were cultured in either IMDM (MV411 only) or RPMI-1640 medium, supplemented with 10% FBS (Peak Serum, Wellington, CO), 100 units/ml penicillin, and 100 μg/ml streptomycin (Life Science Technologies), and 1.0 μg/ml (1.2 μM) vincristine sulfate (dissolved in water). For experiments testing the impact of VCR withdrawal, HL-60/VCR cells were cultured in RPMI-1640 growth medium devoid of vincristine sulfate for 7 days. HL-60 cells were obtained from the ATCC, Manassas, VA. HL-60 daunorubicin resistant cells (HL-60/DNR), grown to tolerate 1.0 μg/ml DNR, were established as previously described[8]; HL-60 and MV411 venetoclax resistant cells (HL-60/VclaxR), established to tolerate 1.0 μM Vclax, were established in a similar fashion.[9] All other cell lines were obtained from ATCC (Manassas, VA). Cell lines were not tested or authenticated over and above documentation provided by ATCC, which included antigen expression, DNA profile, short tandem repeat profiling, and cytogenetic analysis.

2.4 | Cell viability assays

Cell viability was determined by fluorescence measurement as previously described.[11] Briefly, cells were seeded in Corning black wall, 96-well plates (VWR, Suwanee, GA), treated with indicated agents in a final volume of 0.2 ml RPMI-1640 complete medium, and incubated at 37°C, 5% CO_2, for the times indicated. Viability was determined using PI as follows. Cells (positive controls corresponding to 100% cell death) were permeabilized by addition of 10 μl of 1 mg/ml digitonin and incubated at 37°C, 5% CO_2 for 20 min, followed by addition of PI dissolved in PBS, at a final concentration of 5 μM. The plate was incubated for 20 min, and viability was calculated as the mean ($n = 6$) fluorescence (minus non-permeabilized control) at 530 nm excitation and 620 nm emission, using a BIO-TEK Synergy H1 microplate reader (Winooski, VT). Viability was also determined using the MTS Cell Proliferation Assay (Promega), as well as trypan blue (0.4%) exclusion and cell counting on a Countess II apparatus, Life Science Technologies, using disposable hemocytometers, from Invitrogen, Thermo/Fisher Scientific; cell growth rates were assessed by the same method.

2.5 | Caspase activation

Cells (25 000/well) were seeded into Corning white wall, 96-well plates, treated with indicated agents in the final volume of 0.1 ml RPMI-1640 complete medium, and incubated at 37°C, 5% CO_2, for 24 h, after which the cells were exposed to Promega Caspase-Glo® 3/7 Assay mixture (Madison, WI). The plate was incubated at 37°C for 1 h, and caspase activation was calculated as the mean ($n = 8$) luminescence using a BIO-TEK Synergy H1 microplate reader (Winooski, VT).

2.6 | Lipidomics

Lipidomic analysis was conducted using liquid chromatography-electrospray ionization-tandem mass spectrometry (LC-ESI-MS/MS) as previously described.[11] Briefly, total lipids were extracted from cells after the addition of internal standards using ethyl acetate/isopropanol/water (60:30:10, v/v) without phase partitioning. Separation of lipid extracts was achieved using a Waters I-class Acquity LC with a 2.1 × 100 mm C18 CSH column and detected with a Waters Xevo TQ-S MS system.

2.7 | Immunoblotting

Immunoblotting was conducted as previously described[12,13] with modifications. SPHK1 (47 kDa, catalog # 12071), used at 1:1000 dilution, and β-actin (45 kDa, catalog # 3700), used at 1:3000 dilution, were from Cell Signaling. P-gp (180 kDa, catalog # NB60D-1036), used at 1:1000 dilution, was from Novus (Imgenex). GCS (40 kDa, catalog # PA5-42111), used at a 1:1000 dilution, was from Invitrogen. AC (13 kDa, catalog # 612302), used at a 1:1000 dilution, was from Labome (BD Bioscience). Briefly, cells were lysed in 1× RIPA buffer (Cell Signaling Technology, Danvers, MA, USA) containing phosphatase inhibitor cocktail 2, protease inhibitor, and PMSF (1.0 mM; Sigma). The bicinchoninic acid (BCA) method was employed for determining protein concentrations. Lysates were centrifuged to remove debris and then heated in 1× NuPage LDS sample buffer at 95°C for 5 min (GCS lysate was heated at 55°C for 5 min). Equal amounts of total protein were separated by SDS-polyacrylamide gel electrophoresis and subsequently transferred onto PVDF or nitrocellulose membranes (Millipore, Billerica, MA, USA). The membranes were blocked with 5% non-fat milk in PBS for 1 h at room temperature and incubated with primary antibodies according to the dilutions above, at 4°C overnight. The membranes were washed with PBST, followed by incubation with the corresponding HRP-conjugated secondary antibodies, for 1 h at room temperature. The membranes were washed with PBST before exposure. Bound antibodies were measured using an enhanced chemiluminescence detection kit (Thermo Fisher Scientific) and surveyed using a ChemiDoc imaging system (Bio-Rad, Hercules, CA). The relative intensity of protein expression was calculated using ImageJ software (National Institutes of Health).

2.8 | Quantitative reverse transcription PCR (RT-PCR)

An RNA extraction kit (Qiagen Pty., Ltd., Waltham, MA) was used to extract total RNA, which was then reverse-transcribed into cDNA using a ProtoScript II First Strand cDNA Synthesis Kit (New England Biolabs, Ipswich, MA). The synthesized cDNAs were amplified with SYBR Premix (Bimake, Houston, TX) using the ABI VII7 Real-Time PCR

System (Invitrogen). The PCR cycling parameters were 50°C for 2 min and 95°C for 10 min, followed by 40 cycles of 95°C for 15 s and 60°C for 1 min. Relative mRNA levels were calculated using the comparative Ct method (Applied Biosystems instruction manual) and presented as ratios to their biological controls. The fold change in expression of each target mRNA relative to β-actin was calculated as $2^{\Delta(\Delta Ct)}$, where $\Delta Ct = \Delta Ct_{\beta\text{-acin}} - Ct_{genes}$. β-actin transcript levels were confirmed to correlate well with total RNA levels and therefore were used for normalization throughout the experiments.[14,15] The primers used for real-time PCR were designed by primerbank (http://pga.mgh.harvard.edu/primerbank/): (ABCB1: F:TTGCTGCTTACATTCAGGTTTCA, R:AGCCTATCTCCTGTCGCATTA; ABCC1: F: CTCTATCT CTCCCGACATGACC, R: AGCAGACGATCCACAGCA AAA; ABCG2: F: ACGAACGGATTAACAGGGTCA, R: CTCCAGACACACCACGGAT; β-actin: F:GCTGTGCTA CGTCGCCCTG, R:GGAGGAGCTGGAAGCAGCC).

2.9 | Cellular respirometry (intact and permeabilized)

High-resolution O_2 consumption measurements were conducted using the Oroboros Oxygraph-2K (Oroboros Instruments, Innsbruck, Austria) in intact and digitonin permeabilized cells. For each intact cell experiment, cells were centrifuged at 1000 rpm for 7 min at room temperature, washed in PBS, centrifuged once more, and then suspended in assay media at a cell concentration of 2–3 × 10^6 viable cells/ml. Assay media was RPMI 1640, without bicarbonate, supplemented with 20 mM HEPES (pH 7.4), 10% FBS, 100 units/ml penicillin, and 100 μg/ml streptomycin. All experiments were carried out at 37°C in a 1-ml reaction volume. Following the assessment of basal respiration, the following sequential additions were made (oligomycin (5.0 μM), FCCP (0.5, 1, 2, 3 μM), rotenone (Rot; 5 μM), antimycin A (Ant A; 5 μM)). For experiments designed to assess the impact of P-gp, verapamil (10 μM) was added prior to oligomycin to intact cells. For permeabilized cell experiments, cells were centrifuged at 1000 rpm for 7 min at room temperature, washed in respiration buffer, centrifuged once more, and then suspended in respiration buffer at a cell concentration of 2–3 × 10^6 viable cells/ml. Respiration buffer consisted of potassium-MES (105 mM; pH 7.2), KCl (30 mM), KH_2PO_4 (10 mM), $MgCl_2$ (5 mM), EGTA (1 mM), and BSA (2.5 g/L). After recording basal respiration, cells were permeabilized with digitonin (20 μg/ml), energized with various carbon substrates (pyruvate, malate, glutamate, succinate, octanoyl-l-carnitine; P, M, G, S, O; 5, 2, 5, 5, 0.2 mM) and flux was stimulated across a physiological ATP free energy demand using the creatine kinase (CK) clamp, see below for details. Additional respiratory stimulation was carried out via respiratory uncoupler (FCCP) titration (0.5–3.0 μM). Cytochrome C (10 μM) was added to check the integrity of the outer mitochondrial membrane. Note, the absence of an increase in respiration, relative to the pre cytochrome C rate, was used as a quality control assessment for outer membrane integrity. Non-mitochondrial respiration was controlled by adding rotenone (Rot; 5 μM) and/or antimycin A (Ant A; 5 μM). Data were normalized to viable cell count and expressed as pmol/s/million cells. All additions were made directly to the O2K chamber during the period of each assay. Typical assay length was 20–40 min.

2.10 | Mitochondrial isolation

As described previously[16,17] and with some modifications, cells were centrifuged at 300×*g* for 10 min followed by a PBS wash. Cell pellets were resuspended in mitochondrial

isolation buffer (MIB) with BSA (100 mM KCl, 50 mM MOPS, 1 mM EGTA, 5 mM $MgSO_4$, 0.2% BSA, pH 7.1) and homogenized using a borosilicate glass mortar and Teflon pestle. Homogenates were centrifuged at 800×*g* for 10 min at 4°C. The supernatant was collected, and this process was repeated for a total of 3 times. The collected supernatant was centrifuged at 10 000×*g* for 10 min at 4°C to pellet the mitochondrial fraction. The fraction was resuspended in MIB without BSA, transferred to a microcentrifuge tube, and spun down at 10 000×*g*. Final resuspension of the mitochondrial pellet was done in Mitochondria Isolation Buffer, without BSA, and protein concentration was calculated using the Pierce BCA assay. Respiration assays using isolated mitochondria were like that described for permeabilized cells.

2.11 | Mitochondrial functional assessment (isolated mitochondria)

High-resolution O_2 consumption rate (JO_2) measurements were conducted as above. The base assay buffer was identical to that used in permeabilized cells (105 mM potassium-MES, 30 mM KCl, 10 mM KH_2PO_4, 5 mM $MgCl_2$, 1 mM EGTA, 2.5 g/L BSA, and 5 mM creatine monohydrate; pH = 7.2). As previously described,[16,18] a modified version of the CK clamp technique was used to determine steady-state JO_2 across a physiological ΔG_{ATP} span. For complete details regarding the calculation of ΔG_{ATP} at each titration point see.[18] To begin, mitochondria were added to the respiration buffer, followed by the addition of respiratory substrates to stimulate State 4 (i.e., non-phosphorylating) respiration. The CK clamp was then initiated by the addition of ATP (5 mM), PCr (1 mM), and CK (20 U/ml), simulating a “maximal” demand for ATP re-synthesis. Sequential additions of PCr to 6, 15, and 21 mM were then performed to gradually lower the ATP demand state and assess OXPHOS conductance. Four substrate conditions were used: Pyr/M (5/1 mM); glutamate/M (G/M; 10/1 mM); S/Rot (10 mM/0.5 μM); P/M/G/S/O (5/1/5/5/0.2 mM; Multi). For experiments involving dihydroorotate (DHO), DHO (2 mM) was added to isolated mitochondria in the presence of saturating ADP (2 mM). DHO-supported respiration was then inhibited using a specific inhibitor of dihydroorotate dehydrogenase (DHODH), teriflunomide (20 μM). Data were normalized to protein loaded per experiment and then corrected for the mitochondrial enrichment factor (MEF; *) calculated for that sample, with the final values expressed as pmol/s/mg protein* (see proteomics methodology below regarding MEF).

2.12 | Mitochondrial NADH/NAD^+ redox in isolated mitochondria

Fluorescent determination of NADH/NAD^+ was performed using a QuantaMaster Spectrofluorometer (QM-400, Horiba Scientific, Kyoto, Japan). The NADH/NAD+ was detected at Ex/Em: 350/450. NADH/NAD+ was measured in mitochondria using the CK clamp assay. Experiments were performed at 37°C in a 200 μl reaction volume. Mitochondria were incubated at 37°C for ~ 5 min without a substrate to induce a 0% reduction of the NADH pool. Saturating carbon substrates were added (Multi), and respiration was stimulated with the CK clamp. Titration of ΔG_{ATP} was performed via PCr titration (6, 15, 21 mM). Oligomycin (0.02 μM) was added to inhibit ATP synthesis and cyanide (CN, 10 mM) was added to induce a 100% reduction of the matrix NADH pool. The NADH/NAD+ was expressed as a percentage reduction of the CN value (i.e., 100% reduction) based upon the formula % Reduction = $(F–F_{0\%})/(F_{100\%}–F_{0\%}) \times 100$.

2.13 | Mitochondrial H_2O_2 emission

Mitochondrial peroxide emission was assessed in Respiration buffer, supplemented with amplex ultra red (5 μM), horse radish peroxidase (1 U/ml), and superoxide dismutase (25 U/ml), as described previously.[19] Experiments were run in the presence of mitochondria alone, Pyr/M (5/2 mM), and the CK clamp. Relative fluorescence was converted to pmol of H_2O_2 using an H_2O_2 standard curve, as previously described.[19]

2.14 | Mitochondrial lysis and sample prep for label-free proteomics

Isolated mitochondria were lysed in urea lysis buffer (8 M urea in 40 mM Tris, 30 mM NaCl, 1 mM $CaCl_2$, 1× cOmplete ULTRA mini EDTA-free protease inhibitor tablet; pH = 8.0), as described previously.[16,20] The samples were subjected to three freeze-thaw cycles and sonicated with a probe sonicator in three 5s bursts (Q Sonica #CL-188; the amplitude of 30). Samples were centrifuged at 10 000×*g* for 10 min at 4°C. Protein concentration was determined by BCA. Equal amounts of protein were reduced with 5 mM DTT at 37°C for 30 min and then alkylated with 15 mM iodoacetamide for 30 min in the dark at room temperature. Unreacted iodoacetamide was quenched with DTT (15 mm). Initial digestion was performed with Lys C (ThermoFisher Cat# 90307; 1:100 w:w) for 4 h at 37°C. Following dilution to 1.5 M urea with 40 mM Tris (pH = 8.0), 30 mM NaCl, 1 mM $CaCl_2$, samples were digested overnight with trypsin (Promega; Cat# V5113; 50:1 w/w) at 37°C. Samples were acidified to 0.5% TFA and then centrifuged at 4000×*g* for 10 min at 4°C. The supernatant containing soluble peptides was desalted, as described previously[20] and then eluate was frozen and subjected to speedvac vacuum concentration.

2.15 | nLC-MS/MS for label-free proteomics

Final peptides were resuspended in 0.1% formic acid, quantified (ThermoFisher Cat# 23275), and then diluted to a final concentration of 0.25 μg/μl. Samples were subjected to nanoLC-MS/MS analysis using an UltiMate 3000 RSLCnano system (ThermoFisher) coupled to a Q Exactive Plus Hybrid Quadrupole-Orbitrap mass spectrometer (ThermoFisher) via a nanoelectrospray ionization source. For each injection, 4 μL (1 μg) of the sample was first trapped on an Acclaim PepMap 100 20 mm × 0.075 mm trapping column (ThermoFisher Cat# 164535; 5 μl/min at 98/2 v/v water/acetonitrile with 0.1% formic acid). Analytical separation was performed over a 95 min gradient (flow rate of 250 nl/min) of 4%–25% acetonitrile using a 2 μm EASY-Spray PepMap RSLC C18 75 μm × 250 mm column (ThermoFisher Cat# ES802A) with a column temperature of 45°C. MS1 was performed at 70 000 resolution, with an AGC target of 3×10^6 ions and a maximum injection time (IT) of 100 ms. MS2 spectra were collected by data-dependent acquisition (DDA) of the top 15 most abundant precursor ions with a charge greater than 1 per MS1 scan, with dynamic exclusion enabled for 20 s. Precursor ions isolation window was 1.5 *m/z* and the normalized collision energy was 27. MS2 scans were performed at 17 500 resolution, maximum IT of 50 ms, and AGC target of 1×10^5 ions.

2.16 | Data analysis for label-free proteomics

As described previously,[20] with some modification, Proteome Discoverer 2.2 (PDv2.2) was used for raw data analysis, with default search parameters including oxidation (15.995

Da on M) as a variable modification and carbamidomethyl (57.021 Da on C) as a fixed modification. Data were searched against the Uniprot Homo Sapiens reference proteome (Proteome ID: UP000005640), as well as the Human Mito Carta 2.0 database.[21] PSMs were filtered to a 1% FDR and grouped to unique peptides while maintaining a 1% FDR at the peptide level. Peptides were grouped to proteins using the rules of strict parsimony and proteins were filtered to 1% FDR. Peptide quantification was done using the MS1 precursor intensity. Imputation was performed via low abundance resampling. Using only high confidence master proteins, mitochondrial enrichment factor (MEF) was determined as previously described[16] by comparing mitochondrial protein abundance (i.e., proteins identified to be mitochondrial by cross-reference with the MitoCarta 2.0 database) to total protein abundance.

2.17 | Statistical evaluation

All proteomics samples were normalized to total protein abundance, and the protein tab in the PDv2.2 results was exported as a tab delimited .txt. file and analyzed. Protein abundance was converted to the Log_2 space. For pairwise comparisons, tissue mean, standard deviation, *p* value (*p*; two-tailed Student's *t*-test, assuming equal variance), and adjusted *p* value (Benjamini Hochberg FDR correction) were calculated.[22]

Mitochondrial assay results are expressed as the mean ± SEM (error bars). Data were normalized to protein loaded per experiment and then corrected for the mitochondrial enrichment factor (*) calculated for that sample, or the group mean, with the final values expressed as pmol/s/mg protein*. For a detailed description of this method, see previous publication.[16] Throughout the paper, differences between groups were assessed by *t*-test, or one-way ANOVA, followed by Tukey's test where appropriate using GraphPad Prism 8 software (Version 8.4.2). Other statistical tests used are described in the figure legends. Statistical significance in the figures is indicated as follows: *$p < .05$; **$p < .01$; ***$p < .001$; ****$p < .0001$. Unless otherwise stated, figures were generated using GraphPad Prism 8 software (Version 8.4.2) or Biorender.

3 | RESULTS

3.1 | HL-60/VCR cell characteristics

To confirm the VCR resistance status in our model, we determined sensitivity to VCR in wt and in HL-60/VCR cells. As shown, HL-60/VCR cells were near completely refractory to VCR compared to the VCR-naïve, wt counterpart (Figure 1A). From a morphological perspective, wt and VCR-resistant cells were similar in size and appearance; however, HL-60/VCR cells tend to clump in suspension (photos not shown). The cell growth rate was, however, slower in drug-resistant cells compared to wt, with HL-60/VCR growing at 57% the rate of wt cells (Figure 1B). Lastly, and as expected, ABCB1 transcription (P-glycoprotein, P-gp) was markedly elevated (2000-fold) in HL-60/VCR cells along with a slight but significant increase (3-fold) in ABCC1 (MDR protein, MRP), and (25-fold) ABCG2 (breast cancer resistant protein, BCRP) compared to wt cells (Figure 1C).

3.2 | Alterations in SL enzyme expression accompany VCR resistance

Because of the key role that SL's play in cancer growth[23,24] and response to chemotherapy,[25] we were interested in assessing the impact of VCR resistance on the expression of several enzymes involved in SL metabolism. First, the levels of total SPHK1 were elevated in HL-60/VCR cells compared to the wt counterpart (Figure 1D,E). Regarding SPHK1, it is important to note that the product of this enzyme, S1P, is mitogenic, and thus favors neoplastic growth. GCS, which catalyzes glycosylation of ceramide to GC, and in effect dulls ceramide's tumor-suppressor activity by reducing ceramide levels, was overexpressed in VCR-resistant cells (Figure 1D,E). This change in glycosphingolipid metabolism has been shown to accompany MDR.[26] Acid ceramidase (AC) expression was also enhanced in HL-60/VCR compared to wt cells (Figure 1D,E), as previously demonstrated in HL-60/VCR cells.[27] Lastly, although expected, HL-60/VCR cells exhibited markedly elevated levels of P-gp (Figure 1D,E).

3.3 | Lipidomic analysis

Complementary with immunoblot data, HL-60/VCR cells presented with multi-fold increases in S1P and dh-S1P levels, compared to wt cells (Figure 1F); this could be the result of elevated AC activity or reduced S1P lyase expression. Sphingosine levels were similar in both cell lines, whereas the levels of dihydrosphingosine (dhSph), also termed sphinganine, were diminished by approximately 75% in HL-60/VCR cells (Figure 1F). The levels of several ceramide molecular species were increased in HL-60/VCR cells, including C14:0, C16:0, C24:1, as well as the C26 species, C26 and C26:1 (Figure 1G). Although ceramide is proapoptotic, VCR resistance could result in ceramide tolerance that is assisted by enhanced ceramide hydrolysis and glycosylation. Thus, it appears that the increases in ceramide molecular species were mirrored and kept in check by concomitant increases in corresponding GC species, as shown, for example, in C14:0, C16:0, C22:1, C24:1, and C26 molecular species (Figure 1G). Several molecular species of SM were decreased in HL-60/VCR cells versus wt, as demonstrated in C18, C20, C22, and C24 (Figure 1G). On the opposing side, C22:1 SM levels were elevated and a marked increase in C26:1 SM was clearly shown in VCR-resistant cells (Figure 1G). In summary, the data in Figure 1 demonstrate widespread alterations in SL composition occur with VCR resistance, and interestingly, C22:1 ceramide appears to be sequestered in GC and SM. Consistent with a central role for SL metabolism in MDR, SL alterations apparent in HL60/VCR are highly reminiscent to those previously observed in other MDR AML models.[8]

3.4 | Intact cellular respirometry in MDR AML reveals increased mitochondrial content

Mitochondria play a key role in cancer cell biology and are increasingly recognized as potential targets in cancer therapy.[28] Mitochondria are also important downstream targets of ceramide.[29,30] Considering the dynamic changes in SL profiles and enzyme expression patterns that accompanied prior observations in MDR AML and VCR resistance herein,[8] we sought to determine whether mitochondrial metabolism was impacted in the process. To begin, initial respirometry experiments were performed in intact cells under basal conditions, as well as in response to ATP synthase inhibition (i.e., oligomycin), chemical uncoupling (i.e., the addition of the protonophore FCCP), and electron transport inhibition

(i.e., rotenone and antimycin A). Respiration under basal conditions was twofold higher in HL-60/VCR compared to wt cells (Figure 2A, basal abbreviated by "Basal"). Interestingly, the ability of oligomycin to lower respiration was blunted in HL-60/VCR (Figure 2A, "Oligo"). Although inhibition of J_{O_2} by oligomycin is typically interpreted to reflect OXPHOS "coupling efficiency," we hypothesized that high P-gp expression in HL-60/VCR could be driving oligomycin efflux. To test this oligomycin-mediated inhibition of basal respiration was assessed in HL-60/VCR cells in the presence of the P-gp inhibitor verapamil. Under these conditions, oligomycin inhibited basal respiration similar to that seen in wt cell (Figure 2B), confirming P-gp mediated efflux of oligomycin. Maximal uncoupled respiration was nearly twofold higher in HL-60/VCR and respiration remained higher in HL-60/VCR following the addition of both rotenone and antimycin A, suggesting increased non-mitochondrial oxidase activity in HL-60/VCR (Figure 2A, "Rot/Ant"). Correcting for non-mitochondrial J_{O_2}, maximal uncoupled respiration was higher in HL-60/VCR (Figure 2C) consistent with previous findings linking increased mitochondrial content to AML chemoresistance.[2,8] In our model system, HL-60/VCR were continuously cultured in the presence of 1.0 μg/ml (1.2 μM) VCR. To determine if the bioenergetic phenotype observed in VCR resistant cells was attributable to maintaining our stock cultures in VCR medium, we repeated our respirometry experiments in HL-60/VCR cultured in growth media devoid of VCR for seven days. Results revealed nearly identical results to that observed in cells continuously exposed to VCR (Figure 2A, "VCR^{+VCR}" vs "VCR^{-VCR}").

3.5 | Mitochondrial phenotyping in MDR AML reveals intrinsic OXPHOS deficiencies linked to partial CI loss-of-function

Increased basal respiration and higher mitochondrial mass are commonly observed bioenergetic phenotypes associated with MDR.[2,31] Although such phenotypes are presumed to reflect an increased reliance on oxidative ATP production, how the mitochondrial network is intrinsically remodeled to support the MDR phenotype remains poorly understood. To begin to address this gap, we first sought to validate our intact cell respirometry data by directly measuring OXPHOS kinetics in substrate replete permeabilized cells. Surprisingly, despite higher basal respiration (Figure 2D "Cells"), maximal OXPHOS capacity (indicated throughout as $J_{H^+OXPHOS}$) was decreased, rather than increased, in HL-60/VCR cells (Figure 2D). Consistent with this, the ratio of OXPHOS capacity ($J_{H^+OXPHOS}$), to total respiratory capacity (J_{H^+Total})—indicated as Fractional OXPHOS—was reduced nearly twofold in HL60/VCR (Figure 2E). Given that we recently observed low fractional OXPHOS in the setting of venetoclax resistance,[9] we next sought to evaluate both OXPHOS and total respiratory kinetics across multiple MDR AML models. Consistent with data in HL60/VCR, HL60 cells refractory to daunorubicin, as well as MV411 cells refractory to venetoclax all presented with near-identical bioenergetic phenotypes; higher basal respiration and respiratory capacity (Figure 2F,H), lower OXPHOS capacity (Figure 2G,I), and reduced fractional OXPHOS (Figure 2J). Taken together, these data corroborate recent findings[9] and suggest that the combination of increased mitochondrial volume, sufficient to boost both basal and maximal respiratory capacity, along with intrinsic OXPHOS deficiencies are hallmark bioenergetic features of MDR leukemia.

To probe deeper into MDR OXPHOS, we isolated mitochondria from wt and VCR resistant HL-60 cells and evaluated mitochondrial bioenergetic function. Using this workflow, we can further model the impact of a physiological ATP free energy (i.e., ΔG_{ATP}) span on respiratory flux.[18,32] As in the permeabilized cell assay, experimental manipulation of ΔG_{ATP} is made possible via a modified version of the creatine kinase (CK) energetic clamp. This technique leverages the enzymatic activity of CK, which couples the interconversion of ATP and ADP to that of phosphocreatine (PCr) and free creatine (Cr) to titrate the extra-mitochondrial ATP/ADP ratio and allow direct interrogation of OXPHOS kinetics in the presence of various substrate/inhibitor combinations. In isolated mitochondria, respiration assays can then be coupled with parallel measurements of mitochondrial membrane potential and electron reducing the potential to localize OXPHOS deficiencies across distinct bioenergetic nodes.

To begin, isolated mitochondria from wt and VCR resistant HL-60 cells, either continuously exposed to VCR in culture or following 7-day withdrawal, were energized with saturating carbon (pyruvate, malate, glutamate, octanoyl-carnitine, succinate; indicated by “Multi”) and respiration was stimulated with the CK clamp at minimal ATP free energy to mimic maximal OXPHOS demand. Subsequent titrations in PCr were then performed to gradually lower ATP resynthesis. Both maximal respiratory flux and OXPHOS conductance (i.e., the slope of the JO_2 vs ΔG_{ATP} relationship) were decreased in HL-60/VCR (Figure 3A,B). To identify the source of decreased OXPHOS conductance in HL-60/VCR, NADH/NAD^+ redox poise was measured in parallel in substrate-replete isolated mitochondria exposed to an identical ΔG_{ATP} span. Results revealed NADH/NAD^+ hyper-reduction in HL-60/VCR mitochondria (Figure 3C), indicating that OXPHOS impairments in HL-60/VCR are not due to a generalized impairment in dehydrogenase flux, but likely attributable to respiratory complex limitations (i.e., lesions in the electron transport system; ETS).

To investigate complex specific OXPHOS kinetics, mitochondria were energized with either a CI (Pyr/M) or CII (Succ/R) specific substrate combination and respiration was again stimulated with the CK clamp. At minimal ΔG_{ATP}, respiration support by Pyr/M was nearly 2-fold lower in HL-60/VCR (Figure 3D), despite no differences in the presence of S/Rot (Figure 3E). These findings suggested that the respiratory impairments observed with Pyr/M were either caused by limitations in pyruvate uptake/metabolism or due to a generalized impairment in NADH-linked flux (i.e., CI limitations). To distinguish between these possible phenotypes, we performed an additional respirometry assay in which CI-supported flux was fueled with G/M to provide NADH that circumvents pyruvate metabolism (Figure 3F). Under these conditions, G/M supported JO_2 was again reduced in HL-60/VCR (Figure 3F), suggesting a specific bioenergetic limitation localized at CI. In support of this, a dihydroorotate (DHO) assay was performed to provide electrons directly to the ubiquinone pool, thus bypassing CI in a manner comparable to succinate. Respiration supported by DHO was higher in HL-60/VCR (Figure 3G), further corroborating a CI-specific limitation in HL-60/VCR. Interestingly, even in the absence of carbon substrate, mitochondrial respiration was elevated in HL-60/VCR, suggesting the involvement of increased mitochondrial oxidase activity (Figure 3G, “ADP”). To address this, we assessed mitochondrial H_2O_2 emission in deenergized mitochondria, as well as in response to Pyr/M and the CK clamp (Figure 3H,I). Results revealed an over 10-fold increase in

H_2O_2 emission in HL-60/VCR under all conditions (Figure 3H,I). Interestingly, while the addition of the CK clamp decreased peroxide emission in wt mitochondria, presumably as a result of decreased redox pressure, H_2O_2 emission was unaffected by ATP-free energy in HL-60/VCR (Figure 3H,I). Such results are consistent with elevated NAD(P)H oxidase activity in HL-60/VCR mitochondria.

To identify the mechanism of CI deficiency in HL-60/VCR, we conducted a label-free quantitative proteomics screen using peptides prepared from the same isolated mitochondria samples used for functional characterization. In total, we identified 385 differentially expressed mitochondrial proteins (adjusted p value < .01) comparing wt to HL-60/VCR (Table S1). Focusing on the respiratory complexes exclusively, many CI subunits were specifically downregulated in HL-60/VCR (Figure 4A). Interestingly, the core subunits of succinate dehydrogenase (i.e., CII) were increased in HL-60/VCR, presumably to compensate for CI partial loss-of-function (Figure 4A). To explore the biological consequences of CI deficiency in HL-60/VCR, we assessed cell viability in the absence and presence of increasing concentrations of the CI inhibitor, rotenone (Figure 4B,C). Consistent with partial CI loss-of-function, HL-60/VCR cells were found to be highly sensitized to rotenone-induced cytotoxicity (Figure 4C). Taken together, these findings reveal CI deficiency as a previously unidentified bioenergetic vulnerability that accompanies VCR resistance.

3.6 | Forced ceramide accumulation in wt cells phenocopies respiratory complex insufficiency observed with MDR

Pharmacological inhibition of AC, sufficient to increase cellular ceramide molecular species, was recently demonstrated to decrease mitochondrial respiratory competence in drug-resistant AML.[7] Interestingly, respiratory limitations were independent of both carbon substrate and respiratory stimulus and were observed despite no evidence of mitochondrial outer membrane permeabilization. Such findings suggested the intriguing possibility that cellular ceramides may be capable of directly regulating mitochondrial ETS function. In the prior work,[8] as well as herein, AML MDR has been observed to associate with substantial alterations in SL metabolism that center around ceramide detoxification (Figure 1G). Based on this, we hypothesized that OXPHOS deficiency may be consequential to ceramide accumulation in MDR. To determine whether elevated ceramide levels can infringe on mitochondrial function, we grew HL-60 wild-type cells for extended periods (7-days) in a medium containing either C6-ceramide (C6; 10 μM) or ceramide delivered via nanoliposome (CNL; 10 μM), both sources for the production of long-chain ceramides.[33,34] Following 7-days of exposure, mitochondrial OXPHOS kinetics in permeabilized cells was assessed. Despite no change in respiration in the presence of Pyr/M in the absence of adenylate stimulation (Figure 5A; “Pyr/M”), stimulation of near-maximal OXPHOS flux with the CK clamp revealed a near twofold decrease in respiratory flux in cells exposed to both C6 and CNL (Figure 5A; “ΔGATP”). The addition of cytochrome C did not impact respiration, thus confirming functional integrity of the outer mitochondrial membrane across all groups (Figure 5A; “Cyt C”). Relative to vehicle control, respiration remained lower in C6/CNL exposed cells upon addition of glutamate, as well as succinate, following rotenone (Figure 5A; “Succ”). Similar differences in respiration regardless of the carbon substrate

strongly suggest that the respiratory impairments induced by C6/CNL are most likely attributable to ETS dysregulation. Such findings are highly reminiscent of those observed in HL-60/VCR, HL60/DNR, as well as MV411/Vclax (see Figure 2), and thus support a model whereby mitochondrial OXPHOS dysregulation (i.e., low Fractional OXPHOS) may be secondary to altered SL metabolism.

3.7 | Therapeutic synergy induced by co-targeting SL metabolism and respiratory CI in MDR leukemia

Given that sweeping alterations in SL metabolism were observed alongside bioenergetic remodeling in MDR AML, we first sought to explore the synergistic potential of targeting respiratory complex I in conjunction with pharmacological ceramide delivery (e.g., CNL). In these experiments, CI was inhibited using the well-characterized biguanides metformin or phenformin,[35] as well as with the small-molecule IACS-010759.[36] Induction of cellular ceramides was achieved by adding CNL. In HL60/VCR, 48 h exposure to CNL (20 μM), nanoliposome devoid of ceramide (ghost; 20 μM), phenformin (0.5 mM), or phenformin plus ghost had no impact on cell viability (Figure 5B). Remarkably, despite no change in viability for any of the single agents, 48 h exposure to both CNL and phenformin led to a dramatic (>80% of control) decrease in cell viability (Figure 5B). Consistent with this effect, caspase activation was apparent 24 h into CNL/phenformin co-treatment, indicative of apoptotic cell death (Figure 5C). To further the therapeutic efficacy of targeting mitochondrial CI alongside SL metabolism, CNL exposure experiments were repeated in the absence and presence of IACS-010759. Once, again, despite minimal single-agent efficacy, the combination of CNL with IACS-010759 was highly cytotoxic (Figure 5D). Given that alterations in both SL metabolism and mitochondrial bioenergetics were observed herein to be common metabolic features of MRD leukemia, we next sought to investigate the broader therapeutic applications of CNL/phenformin. To do this, we repeated our cell viability assays in the presence of CNL or phenformin, both as single agents and in combination, in HL-60 cells made to be refractory to frontline AML therapies daunorubicin (HL-60/DNR) and venetoclax (HL-60/Vclax), as well as in various other AML cell lines (Kasumi-1, KG-1, THP-1, U937). Of note, both PBMCs from healthy donors, as well as parental HL-60 cells were also included in these experiments (HL-60 wt). Relative to PBMC and across all AML cell lines, despite minimal cytotoxicity as single agents, the combination of CNL and phenformin proved to be remarkably cytotoxic (Figure 5E).

As an alternative strategy to boost cellular ceramides, cell viability experiments, plus and minus metformin/phenformin, were repeated using a variety of SL metabolic inhibitors. These included SK1-i to block SPHK1, SACLAC to block acid ceramidase, and D-threo-PDMP to inhibit GCS.[8,37–41] Except for SK1-i, minimal cytotoxicity was observed in HL-60/VCR cells in the presence of the indicated doses of SACLAC, PDMP, metformin, or phenformin alone (Figure 6A–C). However, the combination of each SL enzyme inhibitor with either metformin or phenformin boosted cytotoxicity, relative to vehicle or single-agent conditions (Figure 6A–C). This relationship was particularly evident for the acid ceramidase inhibitor SACLAC, where relative to the single-agent conditions, the combination of SACLAC and phenformin led to a near 70% decrease in cell viability after only 24 h in both HL60/VCR, as well as wild-type THP-1 (Figure 6C,D). Together, these data

raise the intriguing possibility that co-targeting of cellular sphingolipid metabolism and mitochondrial metabolism, specifically at CI, may represent a novel treatment strategy in difficult to treat MDR leukemia, as well as in wild-type chemotherapy-sensitive phenotypes.

4 | DISCUSSION

A number of studies have been conducted on the relationship of SL's and SL metabolism to chemotherapy resistance, and results have been captioned in excellent works, including reviews.[23,42,43] Gouaze-Andersson and Cabot[44] have reviewed the subject with specific regard to hematological malignancies, and recent work by Snider et al. discloses multiple actions of doxorubicin on SL metabolism in MCF-7 breast cancer cells,[45] including increased levels of S1P and C16 ceramide. In agreement with recent observations in daunorubicin and cytarabine resistant AML,[8] VCR resistance herein was accompanied by substantial alterations in SL composition. The novelty of the present findings stems from our focus on MDR leukemia and its impact on both SL's and mitochondrial function. Moreover, given our recent findings linking SL metabolism to mitochondrial bioenergetics,[7,8] we hypothesized that developing a detailed understanding of the mitochondrial perturbations that accompany the drug-resistant phenotype may reveal new opportunities for targeted therapies that regulate cancer growth. To this end, the present study leveraged a recently described mitochondrial phenotyping platform,[16] specifically designed to evaluate OXPHOS efficiency and capacity, relative to the underlying mitochondrial proteome. Using this platform, we made the exciting discovery that MDR leukemia is accompanied by intrinsic mitochondrial remodeling, typified by increases in a cellular mitochondrial volume sufficient to raise both basal and maximal respiratory capacity. However, contrary to the common assumption associating high basal respiration with enhanced OXPHOS reliance, direct interrogation of the OXPHOS system in MDR leukemia revealed striking OXPHOS limitations. Such limitations are reminiscent of those recently reported in primary AML samples and suggest that the combination of high mitochondrial volume with intrinsic OXPHOS deficiency is advantageous to AML survival.[9] Herein, these changes were subsequently found to sensitize MDR leukemia, as well as chemosensitive AML cell lines, to combinatorial treatment directed at increasing cellular ceramides and further decreasing CI flux within the mitochondria, thus offering an exciting, potential treatment strategy for combatting MDR in the clinic.

With respect to SL metabolism, VCR resistance was accompanied by upregulated expression of SPHK1, GCS, and AC, in addition to the concomitant and expected upregulation of P-gp, a predominant player in MDR.[13] Interestingly, the changes observed in enzyme expression were reflected in the results from lipidomic analyses. For example, increased expression of SPHK1 in HL-60/VCR cells was mirrored by elevated levels of S1P. Overexpression of AC, as noted in HL-60/VCR cells, can also contribute to elevated S1P, as AC liberates sphingosine that is converted to S1P by SPHK1. With regard to ceramide, it is possible that elevated ceramide levels in HL-60/VCR cells resulted from the recycling of sphingosine via the salvage pathway of ceramide synthesis.[46] However, increases in cellular ceramides were countered in part by conversion to GC, a reflection of elevated levels of GCS. High GCS expression and elevated levels of GC have previously been linked to MDR.[26,47–49] As ceramides induce apoptosis, our data suggest that VCR-resistant cells keep levels of

ceramide “in check” via the combined activities of GCS and AC. This is supported by the work of Tan et al[50] and Morad et al[51] who showed that the employ of AC and GCS inhibitors, respectively, in HL-60/VCR cells, increased ceramide levels. Interestingly, even though HL-60/VCR cells contained high levels of S1P, possibly a consequence of S1P lyase deficiency, their growth rate was considerably lower than HL-60 cells. This biology could be related to S1P receptor status in HL-60/VCR cells, as related to work by Van Brocklyn et al on the regulation of proliferation and survival,[52] although this has not been evaluated. We also detected reductions in C18, C20, C22, and C24 molecular species of SM in HL-60/VCR cells, indicative of high sphingomyelinase activity that would contribute to increased ceramide levels. However, only some minor increases in C18, C20, C22, and C24:0 species were detected in the ceramides or in GC. This discrepancy may be a product of altered SL flux.

With regard to P-gp, the bastion of MDR, Gouaze et al., have shown coincidental overexpression of P-gp and GCS in breast cancer and epidermoid carcinoma cells selected for resistance to natural product chemotherapy drugs.[26] Thus, the association of GCS and GC levels with drug resistance[53–55] has a solid footing. Of further relevance, Shabbits and Mayer[56] have shown that ceramide sensitivity in breast cancer cells is modulated by P-gp, and using vincristine as a ceramide generator, Olshefski and Ladisch[6] have shown that GCS inhibition boosts vincristine efficacy.

In addition to changes in SL metabolism, MDR leukemia was accompanied by extensive mitochondrial remodeling. In comparison to wt cells, HL-60/VCR, HL60/DNR, and MV411/Vclax all presented with increases in basal respiration, as well as higher maximal uncoupled oxygen consumption, the latter suggestive of higher mitochondrial content. Increased reliance on mitochondrial metabolism is a commonly emerging theme in cancer drug resistance.[2,3] Although such findings are often interpreted to reflect an increased reliance on oxidative ATP synthesis, it is critical to point out that a large collection of these findings are based solely on measurements of intact cellular respirometry. As demonstrated herein, such methodologies are largely incapable of identifying nuanced bioenergetic inefficiencies across the mitochondrial network in cancer. As such, too much reliance on macro-level changes in cellular bioenergetics (i.e., binary assessments of mitochondrial versus glycolytic “reliance”) may in fact be masking a “goldmine” of cancer-specific mitochondrial biology that if known could potentially be leveraged to develop highly efficacious targeted therapies with a favorable therapeutic index.

Results from experiments in Figures 5 and 6 highlight the integration between SL’s and mitochondrial function and suggest that this link can be exploited therapeutically. For example, with ceramide levels already high in HL-60/VCR cells compared to wild-type (see Figure 1G), the inclusion of either SACLAC or PDMP would be expected to drive ceramide to cytotoxic levels.[8,37,57,58] SK1-i could also backup ceramide levels while limiting S1-P’s mitogenic effects. Interestingly, consequent to baseline disruptions in CI expression, the addition of CI inhibitors metformin or phenformin to the mix likely add “insult to injury,” as amply demonstrated by the synergistic, cytotoxic outcome, most strikingly regarding the CNL-phenformin combination and the SACLAC-phenformin regimen. Moreover, it is noteworthy that we were able to mimic infringement of mitochondrial function typified in

MDR leukemia, by cell supplementation with either C6 or CNL. Given the growing interest in targeting mitochondrial metabolism in cancer,[28] C6/CNL impingement on OXPHOS warrants further investigation.

5 | CONCLUSIONS

In conclusion, increases in SPHK1, GCS, and AC expression that accompany MDR leukemia serve to support cancer cell growth, as the coordinated action of these enzymes may limit the full cancer suppressor actions of ceramide while boosting mitogenicity and leukemic dissemination. Although levels of several ceramide molecular species increased with VCR resistance, a change perhaps favoring apoptosis, it is clear from the lipidomic profiles that VCR-resistant cells endeavor to keep ceramide levels in-check by increasing several GC and SM molecular species. Ceramides may also be of benefit in the induction of autophagy for survival.[59] These factors, in conjunction with the intrinsic mitochondrial remodeling allied with MDR leukemia, promote a resilient cancer phenotype, but also reveal(s) opportunities for the design of novel, targeted therapeutics.[23,60–62] Our approach of leveraging bioenergetic phenotyping to unveil actionable cancer-specific mitochondrial targets holds great potential as a novel drug-discovery platform centered upon mitochondrial precision medicine in MDR that can easily be adapted across cancer types.

Supplementary Material

Refer to Web version on PubMed Central for supplementary material.

Funding information

The work was supported by DOD-W81XWH-19-1-0213 (K.H.F.-W.) and NIH P01 CA171983 (M.C.C), as well as a grant from the Brody Brothers Foundation, Kinston, NC

DATA AVAILABILITY STATEMENT

The datasets generated and/or analyzed during the current study are available in the Open Science Framework (OSF) repository (DOI available on acceptance for publication). For proteomics data, all raw data are available online using accession number “JPST001142” for jPOST Repository [63,64].

Abbreviations

AC	acid ceramidase
AML	acute myeloid leukemia
Ant A	antimycin
CI	complex I
CK	creatine kinase
CN	cyanide

CNL	ceramide nanoliposome
Cyt C	cytochrome c
DHO	dihydroorotate
DNR	daunorubicin
ETS	electron transport system
G	glutamate
GC	glucosylceramides
GCS	glucosylceramide synthase
M	malate
MDR	multidrug resistance
MEF	mitochondrial enrichment factor
Multi	pyruvate/malate/glutamate/succinate/octanoyl-carnitine
O or Oct	octanoyl-carnitine
Oligo	oligomycin
P or Pyr	pyruvate
PBMC	peripheral blood mononuclear cell
PCr	phosphocreatine
Rot	rotenone
S or Succ	succinate
S1P	sphingosine 1-phosphate
SL	sphingolipids
SM	sphingomyelin
SPHK1	sphingosine kinase
TF	teriflunomide
VBL	vinblastine
VCR	vincristine
Vlcax	venetoclax
ΔG_{ATP}	ATP-free energy of hydrolysis

REFERENCES

1. Gottesman MM, Lavi O, Hall MD, Gillet J-P. Toward a better understanding of the complexity of cancer drug resistance. Ann Rev Pharmacol Toxicol. 2016;56:85–102. [PubMed: 26514196]
2. Farge T, Saland E, de Toni F, et al. Chemotherapy-resistant human acute myeloid leukemia cells are not enriched for leukemic stem cells but require oxidative metabolism. Cancer Discov. 2017;7:716–735. [PubMed: 28416471]
3. Guièze R, Liu VM, Rosebrock D, et al. Mitochondrial reprogramming underlies resistance to BCL-2 inhibition in lymphoid malignancies. Cancer Cell. 2019;36:369–384.e13. [PubMed: 31543463]
4. Gu W, Liu T, Fan D, et al. A6 peptide-tagged, ultra-small and reduction-sensitive polymersomal vincristine sulfate as a smart and specific treatment for CD44+ acute myeloid leukemia. J Control Release. 2020;329:706–716. [PubMed: 33031878]
5. Senchenkov A, Litvak DA, Cabot MC. Targeting ceramide metabolism–a strategy for overcoming drug resistance. JNCI J Natl Cancer Inst. 2001;93:347–357. [PubMed: 11238696]
6. Olshefski RS, Ladisch S. Glucosylceramide synthase inhibition enhances vincristine-induced cytotoxicity. Int J Cancer. 2001;93:131–138. [PubMed: 11391632]
7. Fisher-Wellman KH, Hagen JT, Neufer PD, Kassai M, Cabot MC. On the nature of ceramide-mitochondria interactions – dissection using comprehensive mitochondrial phenotyping. Cell Signal. 2021;78:e109838.
8. Kao L-P, Morad SAFF, Davis TS, et al. Chemotherapy selection pressure alters sphingolipid composition and mitochondrial bioenergetics in resistant HL-60 cells. J Lipid Res. 2019;60:1590–1602. [PubMed: 31363040]
9. Nelson MA, McLaughlin KL, Hagen JT, et al. Intrinsic OXPHOS limitations underlie cellular bioenergetics in leukemia. eLife. 2021;10:1–31.
10. Ogretmen B, Safa AR. Identification and characterization of the MDR1 promoter-enhancing factor 1 (MEF1) in the multidrug resistant HL60/VCR human acute myeloid leukemia cell line. Biochemistry. 2000;39:194–204. [PubMed: 10625494]
11. Morad SAF, Ryan TE, Neufer PD, et al. Ceramide-tamoxifen regimen targets bioenergetic elements in acute myelogenous leukemia. J Lipid Res. 2016;57:1231–1242. [PubMed: 27140664]
12. Bartholomae S, Gruhn B, Debatin K-M, et al. Coexpression of multiple ABC-transporters is strongly associated with treatment response in childhood acute myeloid leukemia. Pediatr Blood Cancer. 2016;63:242–247. [PubMed: 26512967]
13. Shaffer BC, Gillet J-P, Patel C, Baer MR, Bates SE, Gottesman MM. Drug resistance: still a daunting challenge to the successful treatment of AML. Drug Resist Updates. 2012;15:62–69.
14. Schmittgen TD, Livak KJ. Analyzing real-time PCR data by the comparative C(T) method. Nat Protoc. 2008;3:1101–1108. [PubMed: 18546601]
15. Nolan T, Hands RE, Bustin SA. Quantification of mRNA using real-time RT-PCR. Nat Protoc. 2006;1:1559–1582. [PubMed: 17406449]
16. McLaughlin KL, Hagen JT, Coalson HS, et al. Novel approach to quantify mitochondrial content and intrinsic bioenergetic efficiency across organs. Sci Rep. 2020;10:17599. [PubMed: 33077793]
17. Nelson MAM, Fisher-Wellman KH. Mitochondrial diagnostics: a discovery-based biochemical platform for phenotyping human peripheral blood cell mitochondria. Methods Mol Biol. 2021;2277:371–389. [PubMed: 34080163]
18. Fisher-Wellman KH, Davidson MT, Narowski TM, Lin C-T, Koves TR, Muoio DM. Mitochondrial diagnostics: a multiplexed assay platform for comprehensive assessment of mitochondrial energy fluxes. Cell Rep. 2018;24:3593–3606.e10. [PubMed: 30257218]
19. Fisher-Wellman KH, Gilliam LAA, Lin C-T, Cathey BL, Lark DS, Darrell Neufer P. Mitochondrial glutathione depletion reveals a novel role for the pyruvate dehydrogenase complex as a key H_2O_2-emitting source under conditions of nutrient overload. Free Radic Biol Med. 2013;65:1201–1208. [PubMed: 24056031]
20. McLaughlin KL, Kew KA, McClung JM, Fisher-Wellman KH. Subcellular proteomics combined with bioenergetic phenotyping reveals protein biomarkers of respiratory insufficiency in the setting of proofreading-deficient mitochondrial polymerase. Sci Rep. 2020;10:3603. [PubMed: 32107436]

21. Calvo SE, Clauser KR, Mootha VK. MitoCarta2.0: an updated inventory of mammalian mitochondrial proteins. Nucleic Acids Res. 2016;44:D1251–D1257. [PubMed: 26450961]
22. Lesack K, Naugler C. An open-source software program for performing Bonferroni and related corrections for multiple comparisons. J Pathol Inform. 2011;2:52. [PubMed: 22276243]
23. Morad SAF, Cabot MC. Ceramide-orchestrated signalling in cancer cells. Nat Rev Cancer. 2013;13:51–65. [PubMed: 23235911]
24. Truman J-P, García-Barros M, Obeid LM, Hannun YA. Evolving concepts in cancer therapy through targeting sphingolipid metabolism. Biochim Biophys Acta. 2014; 1841:1174–1188. [PubMed: 24384461]
25. Morad SAF, Cabot MC. The onus of sphingolipid enzymes in cancer drug resistance. Adv Cancer Res. 2018;140:235–263. [PubMed: 30060811]
26. Gouazé V, Yu JY, Bleicher RJ, et al. Overexpression of glucosylceramide synthase and P-glycoprotein in cancer cells selected for resistance to natural product chemotherapy. Mol Cancer Ther. 2004;3:633–639. [PubMed: 15141021]
27. Tan S-F, Dunton W, Liu X, et al. Acid ceramidase promotes drug resistance in acute myeloid leukemia through NF-κB-dependent P-glycoprotein upregulation. J Lipid Res. 2019;60:1078–1086. [PubMed: 30962310]
28. Vasan K, Werner M, Chandel NS. Mitochondrial metabolism as a target for cancer therapy. Cell Metab. 2020;32:341–352. [PubMed: 32668195]
29. Colombini M Ceramide channels and their role in mitochondria-mediated apoptosis. Biochim Biophys Acta. 2010;1797:1239–1244. [PubMed: 20100454]
30. Neuzil J, Dong L-F, Rohlena J, Truksa J, Ralph SJ. Classification of mitocans, anti-cancer drugs acting on mitochondria. Mitochondrion. 2013;13:199–208. [PubMed: 22846431]
31. Chen J, Kao YR, Sun D, et al. Myelodysplastic syndrome progression to acute myeloid leukemia at the stem cell level. Nat Med. 2019;25:103–110. [PubMed: 30510255]
32. McLaughlin KL, McClung JM, Fisher-Wellman KH. Bioenergetic consequences of compromised mitochondrial DNA repair in the mouse heart. Biochem Biophys Res Commun. 2018;504:742–748. [PubMed: 30217445]
33. Song MS, Posse De Chaves EI. Inhibition of rat sympathetic neuron apoptosis by ceramide. Role of p75NTR in ceramide generation. Neuropharmacology. 2003;45:1130–1150. [PubMed: 14614956]
34. Barth BM, Wang W, Toran PT, et al. Sphingolipid metabolism determines the therapeutic efficacy of nanoliposomal ceramide in acute myeloid leukemia. Blood Adv. 2019;3:2598–2603. [PubMed: 31488436]
35. Bridges HR, Sirviö VA, Agip A-NA, Hirst J. Molecular features of biguanides required for targeting of mitochondrial respiratory complex I and activation of AMP-kinase. BMC Biol. 2016;14:65. [PubMed: 27506389]
36. Molina JR, Sun Y, Protopopova M, et al. An inhibitor of oxidative phosphorylation exploits cancer vulnerability. Nat Med. 2018;24:1036–1046. [PubMed: 29892070]
37. Pearson JM, Tan SF, Sharma A, et al. Ceramide analogue SACLAC modulates sphingolipid levels and MCL-1 splicing to induce apoptosis in acute myeloid leukemia. Mol Cancer Res. 2020;18:352–363. [PubMed: 31744877]
38. Chatzakos V, Rundlöf AK, Ahmed D, De Verdier PJ, Flygare J. Inhibition of sphingosine kinase 1 enhances cytotoxicity, ceramide levels and ROS formation in liver cancer cells treated with selenite. Biochem Pharmacol. 2012;84:712–721. [PubMed: 22727936]
39. Maurer BJ, Melton L, Billups C, Cabot MC, Reynolds CP. Synergistic cytotoxicity in solid tumor cell lines between N-(4-hydroxyphenyl)retinamide and modulators of ceramide metabolism. J Natl Cancer Inst. 2000;92:1897–1909. [PubMed: 11106681]
40. Yang YL, Ji C, Cheng L, et al. Sphingosine kinase-1 inhibition sensitizes curcumin-induced growth inhibition and apoptosis in ovarian cancer cells. Cancer Sci. 2012;103:1538–1545. [PubMed: 22594559]
41. Huang W, Tsai C, Chen C, et al. Glucosylceramide synthase inhibitor PDMP sensitizes chronic myeloid leukemia T315I mutant to Bcr-Abl inhibitor and cooperatively induces glycogen synthase kinase-3-regulated apoptosis. FASEB J. 2011;25:3661–3673. [PubMed: 21705667]

42. Giussani P, Tringali C, Riboni L, Viani P, Venerando B. Sphingolipids: key regulators of apoptosis and pivotal players in cancer drug resistance. Int J Mol Sci. 2014;15:4356–4392. [PubMed: 24625663]
43. Lee W-K, Kolesnick RN. Sphingolipid abnormalities in cancer multidrug resistance: chicken or egg? Cell Signal. 2017;38:134–145. [PubMed: 28687494]
44. Gouaze-Andersson V, Cabot MC. Sphingolipid metabolism and drug resistance in hematological malignancies. Anticancer Agents Med Chem. 2011;11:891–903. [PubMed: 21707483]
45. Snider JM, Trayssac M, Clarke CJ, et al. Multiple actions of doxorubicin on the sphingolipid network revealed by flux analysis. J Lipid Res. 2019;60:819–831. [PubMed: 30573560]
46. Kitatani K, Idkowiak-Baldys J, Hannun YA. The sphingolipid salvage pathway in ceramide metabolism and signaling. Cell Signal. 2008;20:1010–1018. [PubMed: 18191382]
47. Gouazé-Andersson V, Yu JY, Kreitenberg AJ, Bielawska A, Giuliano AE, Cabot MC. Ceramide and glucosylceramide upregulate expression of the multidrug resistance gene MDR1 in cancer cells. Biochim Biophys Acta. 2007;1771:1407–1417. [PubMed: 18035065]
48. Messner MC, Cabot MC. Glucosylceramide in humans. Adv Exp Med Biol. 2010;688:156–164. [PubMed: 20919653]
49. Liu YY, Patwardhan GA, Xie P, Gu X, Giuliano AE, Cabot MC. Glucosylceramide synthase, a factor in modulating drug resistance, is overexpressed in metastatic breast carcinoma. Int J Oncol. 2011;39:425–431. [PubMed: 21617856]
50. Tan S-F, Liu X, Fox TE, et al. Acid ceramidase is upregulated in AML and represents a novel therapeutic target. Oncotarget. 2016;7:83208–83222. [PubMed: 27825124]
51. Morad SAFF, Tan S-F, Feith DJ, et al. Modification of sphingolipid metabolism by tamoxifen and N-desmethyltamoxifen in acute myelogenous leukemia–impact on enzyme activity and response to cytotoxics. Biochim Biophys Acta. 2015;1851:919–928. [PubMed: 25769964]
52. Van Brocklyn JR, Lee M-J, Menzeleev R, et al. Dual actions of sphingosine-1-phosphate: extracellular through the Gi-coupled receptor Edg-1 and intracellular to regulate proliferation and survival. J Cell Biol. 1998;142:229–240. [PubMed: 9660876]
53. Lavie Y, Cao H, Bursten SL, Giuliano AE, Cabot MC. Accumulation of glucosylceramides in multidrug-resistant cancer cells. J Biol Chem. 1996;271:19530–19536. [PubMed: 8702646]
54. Lucci A, Cho WI, Han TY, Giuliano AE, Morton DL, Cabot MC. Glucosylceramide: a marker for multiple-drug resistant cancers. Anticancer Res. 1998;18:475–480. [PubMed: 9568165]
55. Liu YY, Han TY, Giuliano AE, Cabot MC. Ceramide glycosylation potentiates cellular multidrug resistance. FASEB J. 2001;15:719–730. [PubMed: 11259390]
56. Shabbits JA, Mayer LD. P-glycoprotein modulates ceramide-mediated sensitivity of human breast cancer cells to tubulin-binding anticancer drugs. Mol Cancer Ther. 2002;1:205–213. [PubMed: 12467215]
57. Baran Y, Bielawski J, Gunduz U, Ogretmen B. Targeting glucosylceramide synthase sensitizes imatinib-resistant chronic myeloid leukemia cells via endogenous ceramide accumulation. J Cancer Res Clin Oncol. 2011;137:1535–1544. [PubMed: 21833718]
58. Yamane M, Miyazawa K, Moriya S, Abe A, Yamane SD, L-Threo-1-phenyl-2-decanoylamino-3-morpholino-1-propanol (DL-PDMP) increases endoplasmic reticulum stress, autophagy and apoptosis accompanying ceramide accumulation via ceramide synthase 5 protein expression in A549 cells. Biochimie. 2011;93:1446–1459. [PubMed: 21571032]
59. Jiang W, Ogretmen B. Autophagy paradox and ceramide. Biochim Biophys Acta—Mol Cell Biol Lipids. 2014;1841:783–792.
60. Bonhoure E, Pchejetski D, Aouali N, et al. Overcoming MDR-associated chemoresistance in HL-60 acute myeloid leukemia cells by targeting sphingosine kinase-1. Leukemia. 2006;20:95–102. [PubMed: 16281067]
61. Paugh SW, Paugh BS, Rahmani M, et al. A selective sphingosine kinase 1 inhibitor integrates multiple molecular therapeutic targets in human leukemia. Blood. 2008;112:1382–1391. [PubMed: 18511810]
62. Ogretmen B Sphingolipid metabolism in cancer signalling and therapy. Nat Rev Cancer. 2018;18:33–50. [PubMed: 29147025]

63. Okuda S, Watanabe Y, Moriya Y, et al. jPOSTrepo: an international standard data repository for proteomes. Nucleic Acids Res. 2017;45:D1107–D1111. [PubMed: 27899654]

64. Deutsch EW, Csordas A, Sun Z, et al. The ProteomeXchange consortium in 2017: supporting the cultural change in proteomics public data deposition. Nucleic Acids Res. 2017;45:D1100–D1106. [PubMed: 27924013]

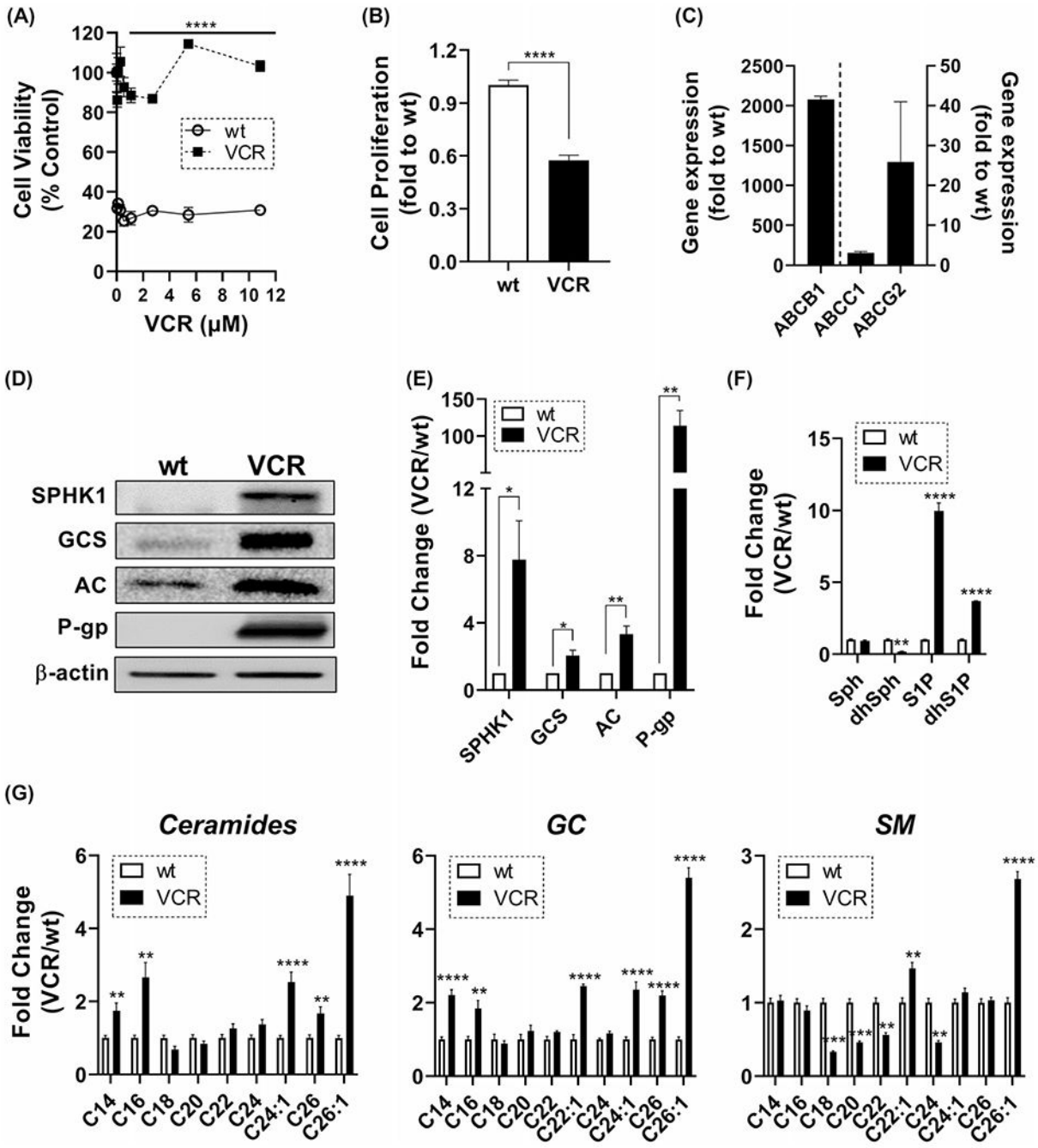

FIGURE 1.

Alterations in sphingolipid metabolism underlie vincristine (VCR) resistance in HL-60 cells. (A) VCR cytotoxicity. HL-60 and HL-60/VCR cells were seeded in 96-well plates (50 000 cells/well) and exposed to VCR concentrations indicated for 48 h. Viability was determined by MTS assay. (B) Cell growth rates determined by viable cell counts. VCR was present in HL-60/VCR growth medium. (C) ABC transporter gene expression profile. Changes in gene expression in HL-60/VCR cells are represented as fold-increase over levels measured in wt cells. (D) Representative immunoblots for SPHK1, GCS, AC, P-gp, and β-actin.

(E) Immunoblot quantification represented by fold-increases in blot density over wt. (F) Long-chain bases and S1P profiles. (G) Ceramide, GC, and SM molecular species profiled in wt and HL-60/VCR cells. Figures generated using GraphPad Prism 8 software (Version 8.4.2). Data are Mean ± SEM, (A,B) $N = 6$/group, (C–F) $N = 3$/group, (G) $N = 4–7$/group. *$p < .05$, **$p < .01$, ***$p < .001$, ****$p < .0001$

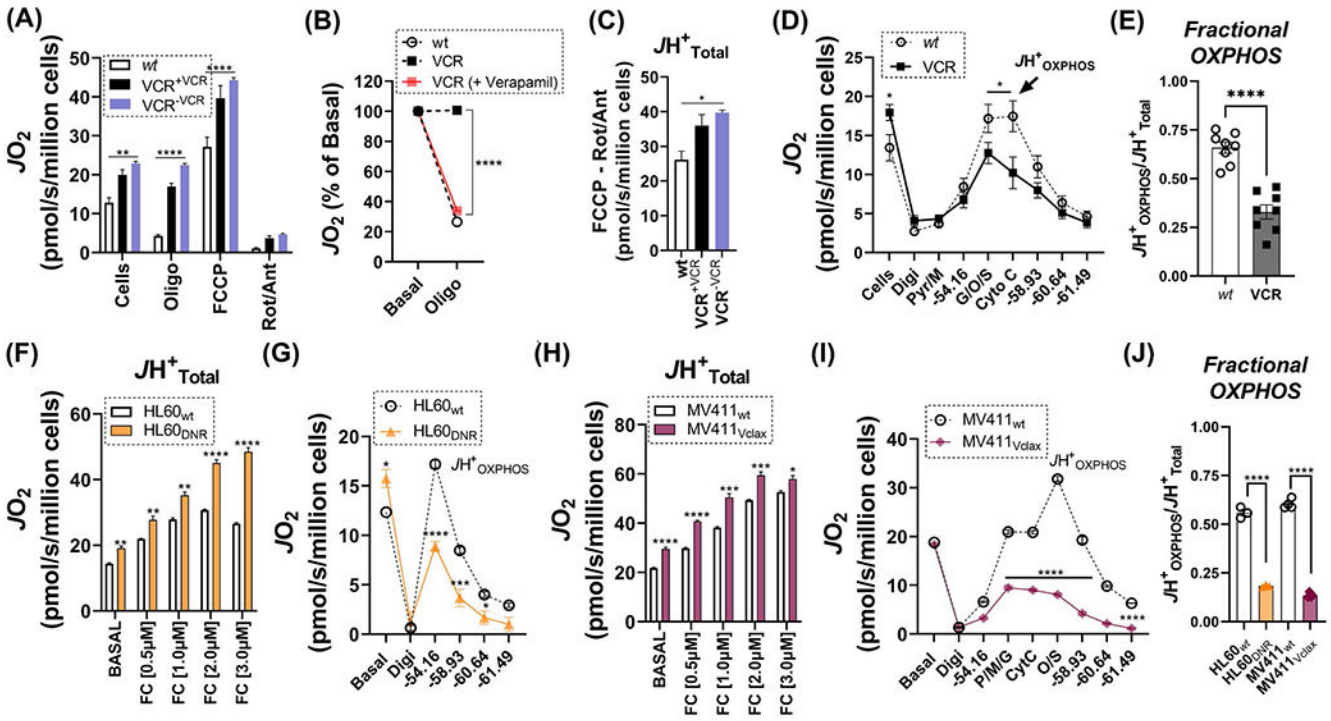

FIGURE 2.

Increased basal and maximal respiration along with low fractional oxidative phosphorylation (OXPHOS) characterizes multidrug resistance leukemia. (A) Oxygen consumption in intact HL-60 wt and HL-60/VCR cells under basal conditions, as well as following the addition of oligomycin (Oligo), FCCP (max rate depicted based on titrations of 0.5, 1, 2, and 3μM), rotenone (Rot), and antimycin A (Ant). (B) Percent decrease in basal respiration induced by oligomycin in wt cells, as well as vehicle or verapamil (10 μM)-treated HL-60/VCR cells. (C) FCCP stimulated respiration corrected for oxygen consumption remaining following rotenone/antimycin. Indicated throughout as total respiratory capacity —$\mathit{J}H^{+}_{Total}$. (D) Oxygen consumption in digitonin (0.02 mg/ml) permeabilized cells in the absence of substrates (Digi), as well as following the addition of P/M (5 mM/1 mM), ATP-free energy (−54.16 kJ/mol), additional substrate G/O/S (5 mM/0.2 mM/5 mM), cytochrome C (Cyt), phosphocreatine titration to manipulate ATP-free energy. Data displayed were corrected for respiration remaining following Rot/Ant. Maximal respiration in the presence of saturating substrate and minimal ATP-free energy was denoted as maximal OXPHOS flux (i.e., $\mathit{J}H^{+}_{oxphos}$). (E) Ratio of $\mathit{J}H^{+}_{oxphos}$ to $\mathit{J}H^{+}_{Total}$—Fractional OXPHOS. (F) Intact cellular respiration to assess basal and $\mathit{J}H^{+}_{Total}$ in wildtype HL-60 and $HL60_{DNR}$. (G) OXPHOS kinetics assay, like panel D. (H) Intact cellular respiration to assess basal and $\mathit{J}H^{+}_{Total}$ in wildtype MV411 and $MV411_{Vclax}$. (I) OXPHOS kinetics assay, like panel D. (J) Calculated Fractional OXPHOS. Figures generated using GraphPad Prism 8 software (Version 8.4.2). Data are Mean ± SEM, (A, B, D, E) N = 4–10/group, (C, F–J) N = 3–5/group. *p < .05, **p < .01, ***p < .001, ****p < .0001

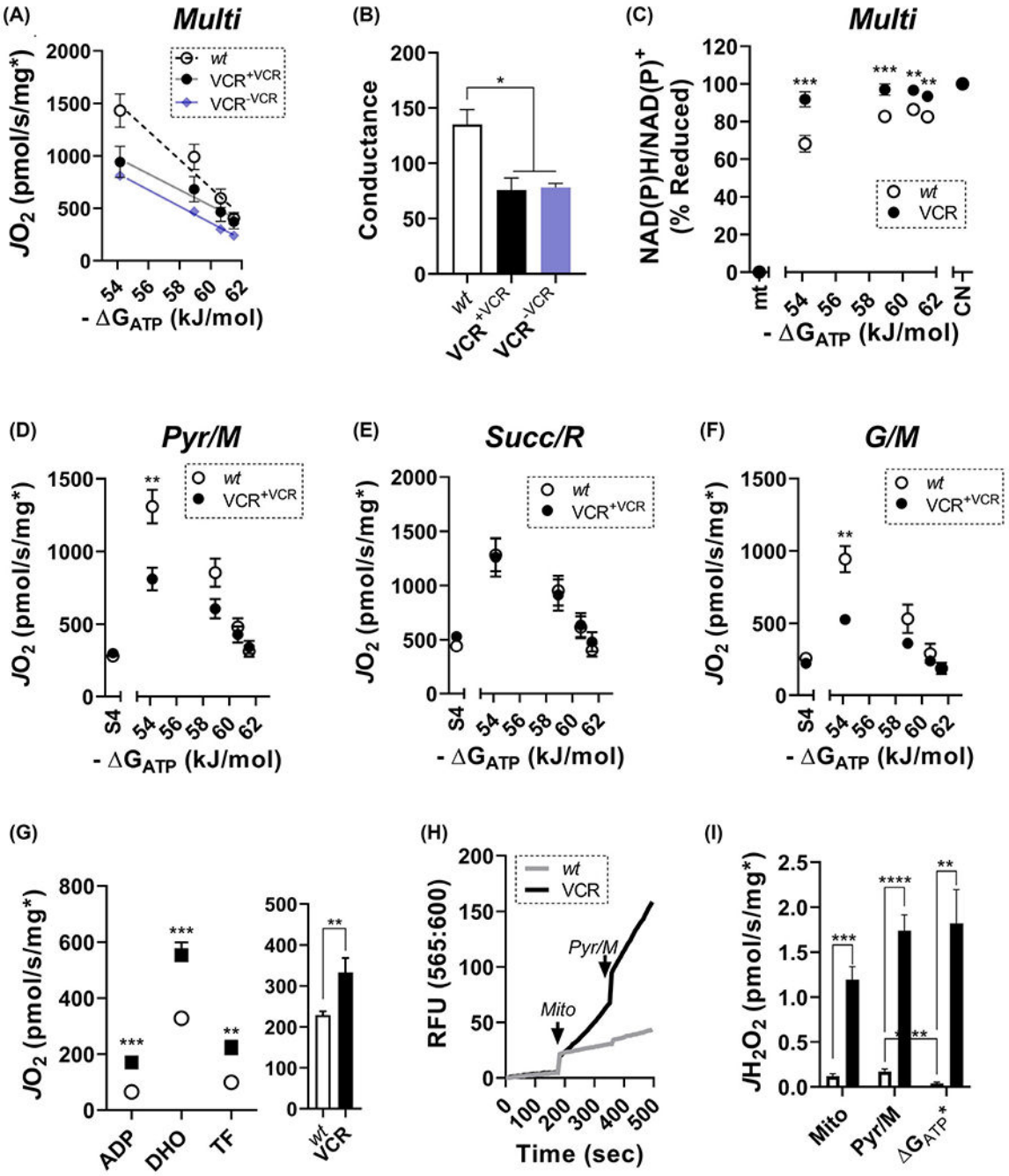

FIGURE 3.

Mitochondrial phenotyping links low fractional oxidative phosphorylation to CI partial loss-of-function. All experiments were performed in isolated mitochondria. (A) Relationship between JO_2 and ATP-free energy (ΔG_{ATP}) clamped with the CK clamp in mitochondria energized with Multi. (B) Respiratory conductance—the slope of the relationship between JO_2 and ΔG_{ATP}. (C) Relationship between NAD(P)H/NAD(P)$^+$ redox and ATP-free energy (ΔG_{ATP}) clamped with the CK clamp in mitochondria energized with Multi. (D–F) Relationship between JO_2 and ATP-free energy (ΔG_{ATP}) clamped with the CK clamp

in mitochondria energized with Pyr/M, Succ/R, and G/M. (G) Respiration experiments in mitochondria exposed to saturating ADP, followed by the addition of DHO, and teriflunomide. Bar graph inset displays DHO-specific flux calculated from comparing respiration in the presence of DHO minus that observed in the presence of teriflunomide. (H) Representative trace of a mitochondrial H_2O_2 emission experiment in wt and HL-60/VCR mitochondria. Data depict fluorescence in response to mitochondrial addition, as well as Pyr/M. (I) Quantified mitochondrial H_2O_2 emission. (A–I) Data normalized to protein corrected for each sample's mitochondrial enrichment factor (MEF), assessed via nLC-MS/MS (see methods). Figures generated using GraphPad Prism 8 software (Version 8.4.2). Data are Mean ± SEM, (A–C) $N = 3–11$/group, (D–E) $N = 9–10$/group, (F) $N = 4$/group, (G) $N = 7–8$/group, (I) $N = 5$/group. *$p < .05$, **$p < .01$, ***$p < .001$, ****$p < .0001$

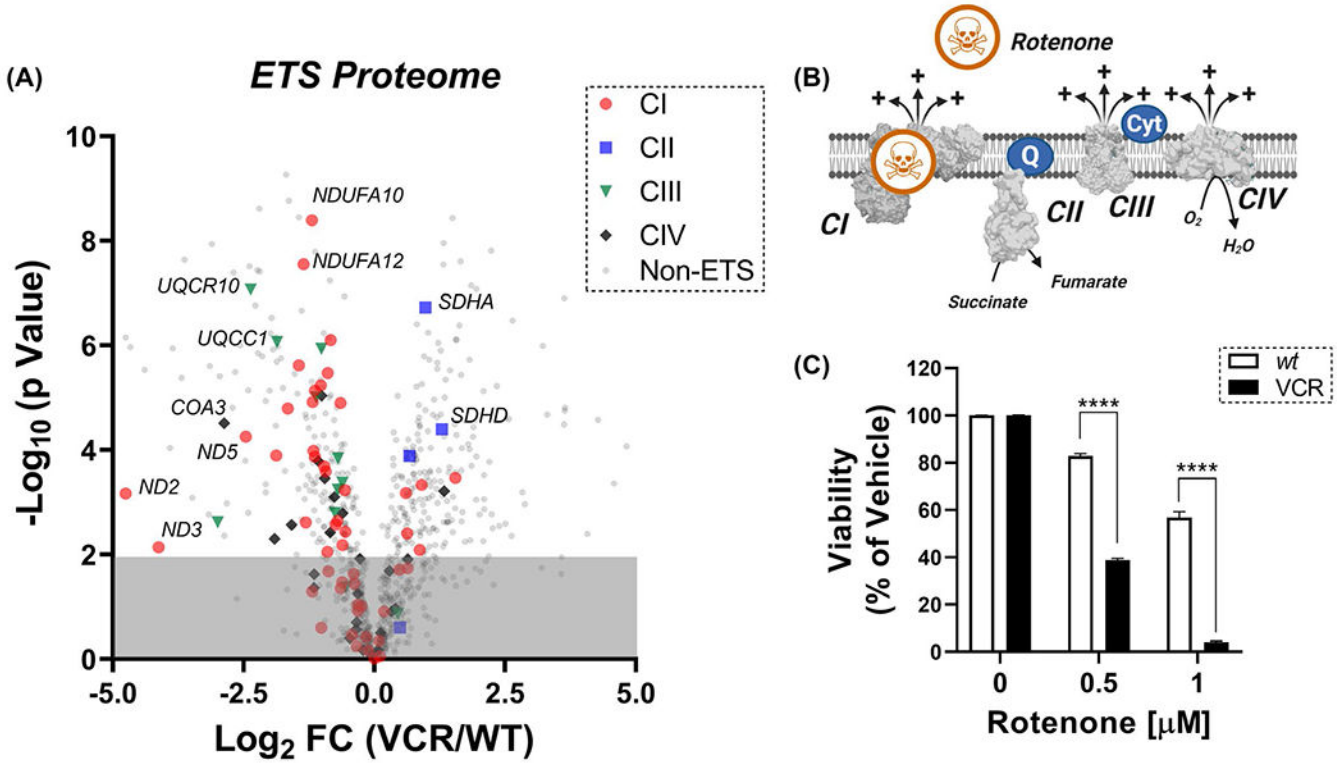

FIGURE 4.

Decreased CI expression underlies vincristine (VCR) resistance. (A) Label-free nLC-MS/MS was performed on mitochondrial lysates from each sample. Volcano plot depicting changes in the mitochondrial proteome between HL-60/VCR and wt. Protein subunits of each respiratory complex (CI, CII, CIII, CIV) are indicated by color. (B) Cartoon depicting CI inhibition by rotenone. (C) Cell viability in response to 24 h of exposure to increasing concentrations of rotenone in wt and HL-60/VCR cells. Viability assessed via counting in the presence of trypan blue. Figures generated using GraphPad Prism 8 software (Version 8.4.2) and Biorender. Data are Mean ± SEM, (A) $N = 5$/group, (C) $N = 6$/group. *$p < .05$, **$p < .01$, ***$p < .001$, ****$p < .0001$

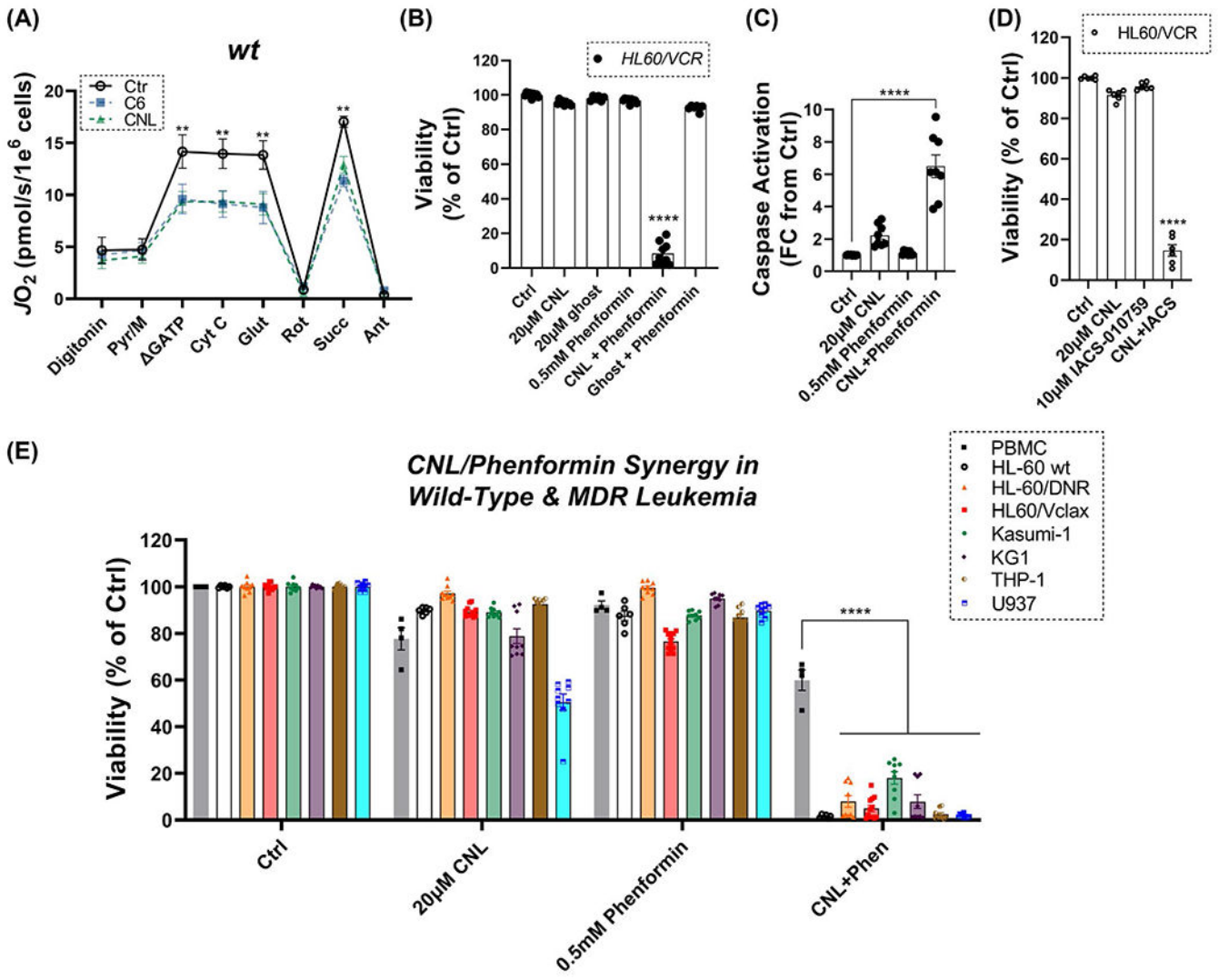

FIGURE 5.

Mitochondrial CI inhibition in conjunction with administration of short-chain nanoliposomal ceramide results in synergistic cytotoxicity. (A) Respiration in permeabilized HL-60 wt cells following exposure to vehicle C6 (10 μM) or CNL (10 μM) for 7-days. Cells were permeabilized with digitonin (0.02 mg/ml) and respiration was assessed in response to the indicated additions. Data normalized to viable cell count. (B–D) All experiments were done in HL-60/VCR cells. (B) Cell viability, determined by viable cell count, in HL-60/VCR cells exposed for 48h to CNL (20 μM), ghost (20 μM), phenformin (0.5 mM), CNL (20 μM) + phenformin (0.5 mM), or ghost (20 μM) + phenformin (0.5 mM). (C) Caspase activation in HL-60/VCR cells exposed for 24 h to vehicle (Ctrl), CNL (20 μM), phenformin (0.5 mM), or CNL (20 μM) + phenformin (0.5 mM). (D) Cell viability in response to 48 h of exposure to either CNL (20 μM), IACS-010759 (10 μM), or CNL (20 μM) + IACS-010759 (10 μM). (E) Cell viability, determined by viable cell count, in PBMC, HL-60 wt, HL-60/DNR, HL-60/Vclax, Kasumi-1, KG-1, THP-1, and U937 cells exposed for 48 h to vehicle (Ctrl), CNL (20 μM), phenformin (0.5 mM), or CNL (20 μM) + phenformin (0.5 mM). Viability

assessed via counting in the presence of trypan blue. Figures generated using GraphPad Prism 8 software (Version 8.4.2). Data are Mean ± SEM, (A) $N = 3$/group, (B–E) $N = 6–12$/group. *$p < .05$, **$p < .01$, ***$p < .001$, ****$p < .0001$

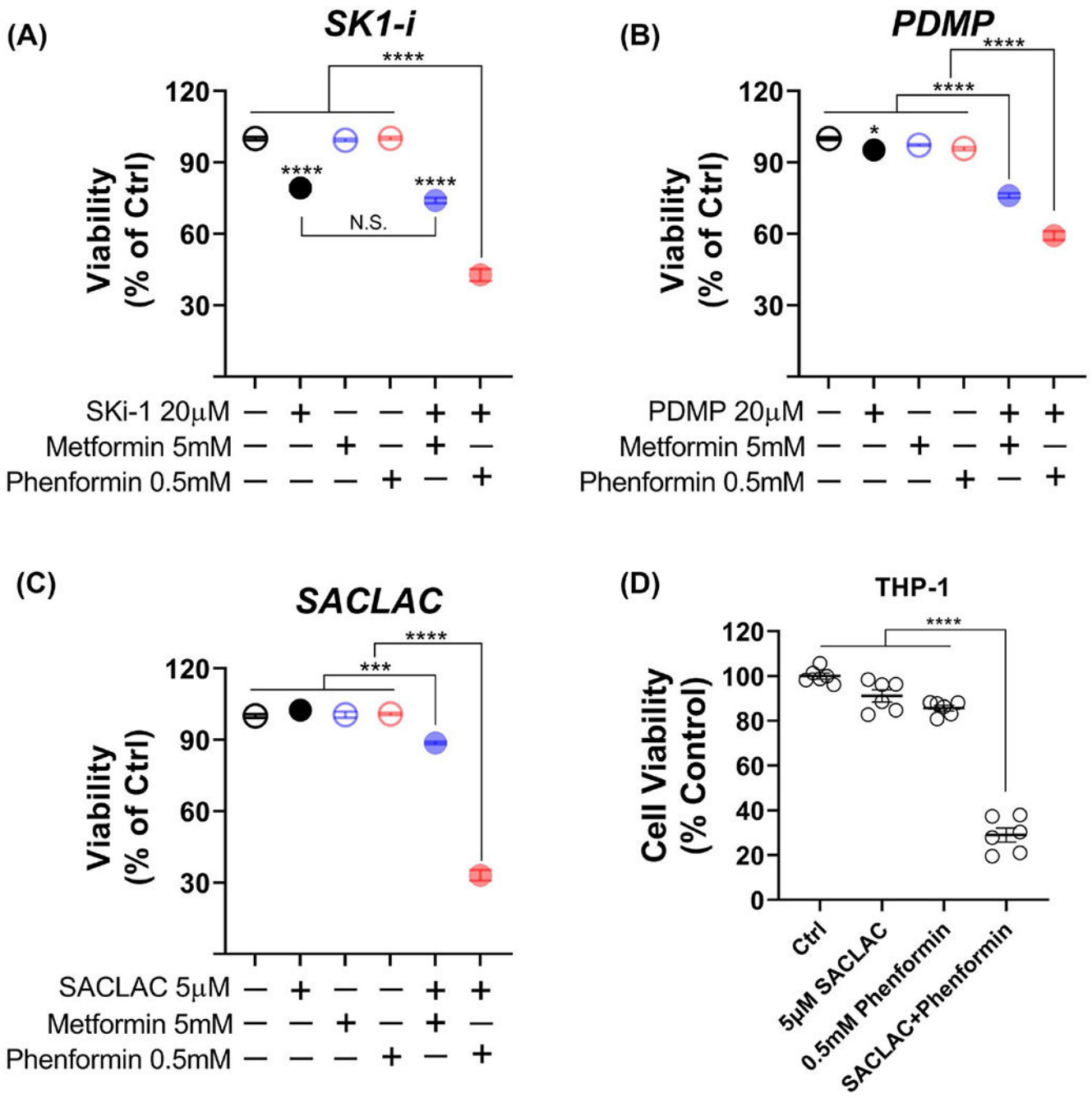

FIGURE 6.

Co-targeting of respiratory CI and enzymes of sphingolipid metabolism induces synergistic cytotoxicity. (A–C) Experiments performed in HL60/VCR. Cell viability in response to 24 h of exposure to Ski-1 (20 μM), 1-phenyl-2-decanoylamino-3-morpholino-1-propanol (PDMP) (20 μM), SACLAC (5 μM), metformin (5 mM) or phenformin (0.5 mM). Metformin and phenformin were administered alone or in combination with Ski-1, PDMP, or SACLAC. Viability assessed via counting in the presence of trypan blue. (D) Cell viability in THP-1 cells treated with vehicle, SACLAC (5 μM), phenformin (0.5 mM), or SACLAC

+ phenformin. Figures generated using GraphPad Prism 8 software (Version 8.4.2). Data are Mean ± SEM, (A–D) $N = 3–6$/group. *$p < .05$, **$p < .01$, ***$p < .001$, ****$p < .0001$